Static atomic displacements in Cu-Mn measured with diffuse x-ray scattering

B. Schönfeld,[1,2] H. Roelofs,[1,*] G. Kostorz,[1] J. L. Robertson,[3] P. Zschack,[4] and G. E. Ice[3]
[1]*Department of Physics, ETH Zurich, 8093 Zurich, Switzerland*
[2]*Department of Materials, Laboratory of Metal Physics and Technology, ETH Zurich, 8093 Zurich, Switzerland*
[3]*Materials Science and Technology Division, Oak Ridge National Laboratory, Oak Ridge, Tennessee 37831, USA*
[4]*Advanced Photon Source, Argonne National Laboratory, Argonne, Illinois 60439, USA*
(Received 1 August 2007; revised manuscript received 2 November 2007; published 3 April 2008)

Diffuse x-ray scattering of a Cu-17.2 at. % Mn single crystal, which was aged at 483 K for 2 weeks, was taken at three energies, namely, 6526, 8969, and 8909 eV, which were suited for an evaluation by the 3λ technique. The values of the species-dependent static atomic displacements closely agree with those of a Georgopoulos–Cohen evaluation, which also uses the three data sets. Nearest-neighbor displacements are dominant and with ~0.038 Å largest among Cu-Mn pairs. A tendency is noted for lattice expansion between those elements (equal or unequal pairs) that are preferred in site occupancy over a random arrangement because of local atomic order.

DOI: 10.1103/PhysRevB.77.144202 PACS number(s): 61.66.Dk, 64.60.Cn

I. INTRODUCTION

Cu-Mn has been repeatedly investigated for chemical and magnetic atomic short-range order (see, e.g., Roelofs *et al.*[1] and references therein). By employing wide-angle and small-angle scattering of neutrons, a correlation between the degree of local atomic order and the tendency for ferromagnetic order below the spin-glass temperature was established, while the antiferromagnetic character of the spin glass was found to be robust against changes in the degree of chemical local order.[2,3] For a comprehensive description of the local atomic arrangement in this alloy, knowledge of the static atomic displacements is still missing. Because of the atomic scattering factor variation, x-ray diffuse scattering offers a more suitable tool to extract static atomic displacements. Knowledge about displacements may be of additional interest for two reasons. (i) The strain-induced (or elastic) part in the effective pair interaction parameters was invoked to account for a nonanalytical behavior at the Γ position.[4] While this behavior was deduced from high-energy x-ray measurements, a subsequent experimental investigation by small-angle neutron scattering was unable to show the expected features.[5] (ii) In a comprehensive study of Gödecke (see Ref. 6 and references therein), anomalies in the temperature dependence of macroscopic properties (dilatation, elastic modulus, and electric resistivity) were noted and interpreted as transitions between different phases (Cu_5Mn and Cu_3Mn). The presence of such superstructures, however, was not supported on the basis of local atomic order.[1,7–9] Still, static displacements may indicate such a tendency.

Species-dependent static atomic displacements may be obtained from diffuse x-ray scattering. Here, two procedures are applied, i.e., the so-called reciprocal-space approach and the real-space approach. The reciprocal-space approach[10] is most suited for dilute alloys as it supplies the long-ranging displacement field due to defects within the matrix based on the single-defect approximation. Recently, this method was applied to concentrated alloys,[4] which implied the loss of an inherent species dependence in the displacements.[11] For the real-space approach, two procedures are currently followed with binary alloys *A*-*B* if one wants to separate the 25 Fourier series representing the elastic scattering contributions in an expansion up to second order in the displacement scattering. (i) When measurements are performed at a conventional x-ray source using a single x-ray energy, the Georgopoulos–Cohen method[12] (an extension of the earlier Borie–Sparks evaluation scheme,[13] which is valid for neutron scattering) is applied. As correlations between the *A*-*A* and *B*-*B* displacements are strong, a stabilization technique such as the ridge-regression method has to be applied. (ii) The 3λ method introduced by Ice *et al.*[14] offers the advantage of reducing the number of unknown Fourier series from 25 to 7. This is achieved by an additional "null-Laue" measurement where the scattering contrast of the alloying partners is tuned to (approximately) zero, and scattering then comprises (nearly) exclusively static quadratic displacement scattering together with thermal diffuse scattering and Compton scattering. The second measurement is performed close to the absorption edge of the constituent that will provide the largest scattering contrast. A combination of these two measurements already allows the leading Fourier coefficients of local order and the species-dependent displacements to be separated, which is similar to a Georgopoulos–Cohen analysis. The separation, however, is strongly stabilized by increasing the variation of the scattering contrast through a third measurement close to the absorption edge of the other constituent.

The 3λ method works well if the alloy consists of elements that are near neighbors in the periodic table. Such investigations were performed for Ni-Fe,[15,16] Fe-Cr,[17] and Ni-Cr alloys.[18] For the latter two investigations, a comparison between the Georgopoulos–Cohen and the 3λ evaluation was performed;[18,19] while an excellent agreement was observed for Fe-Cr, larger differences were seen in Ni-Cr. It seemed appropriate to perform such a comparative study also for Cu-Mn, i.e., a system where the atomic numbers of the alloying partners also differ by four (such as in Ni-Cr). A state already well characterized by neutron scattering was chosen because it offers high-precision data in short-range order and (effective) displacement scattering as a reference (the different signs of the coherent scattering lengths of Cu and Mn lead to a large scattering contrast).

 ©2008 The American Physical Society

II. THEORY

The elastic diffuse scattering from a binary cubic alloy (A-B) is usually separated into three contributions, namely, short-range order scattering, linear displacement scattering, and Huang scattering[12,13] (for the nomenclature, see Ref. 19). While short-range order scattering comprises one Fourier series,

$$I_{\mathrm{SRO}}(\mathbf{h}) = \sum_{l,m,n} \alpha_{lmn} \cos \pi h_1 l \cos \pi h_2 m \cos \pi h_3 n, \quad (1)$$

linear displacement scattering is characterized by six Fourier series $Q_i^{\mu\mu}(\mathbf{h})$, with $\mu = A, B$ and $i = x, y, z$, e.g.,

$$Q_x^{AA}(\mathbf{h}) = -2\pi \sum_{l,m,n} (c_A/c_B + \alpha_{lmn}) \times \langle x_{lmn}^{AA} \rangle \sin \pi h_1 l \cos \pi h_2 m \cos \pi h_3 n,$$

$$Q_x^{BB}(\mathbf{h}) = 2\pi \sum_{l,m,n} (c_B/c_A + \alpha_{lmn}) \times \langle x_{lmn}^{BB} \rangle \sin \pi h_1 l \cos \pi h_2 m \cos \pi h_3 n. \quad (2)$$

Here, $\mathbf{h} = (h_1, h_2, h_3)$ is the scattering vector in reciprocal lattice units (rlu), (l, m, n) defines the neighboring shell (sites in units of half the lattice parameter), α_{lmn} are the Warren–Cowley short-range order parameters, c_μ are the atomic fractions of component μ, and $\langle x_{lmn}^{\mu\mu} \rangle$ are the averaged static atomic displacements between μ-μ pairs in units of the lattice parameter a. All three displacements $\langle x_{lmn}^{\mu\nu} \rangle$ when weighted with their abundance must sum up to zero for any neighboring shell lmn as there is an average lattice.

Within the linear approximation of the displacement scattering, the elastic diffuse scattering $I_{\mathrm{diff}}(\mathbf{h})$ in electron units reads

$$I_{\mathrm{diff}}(\mathbf{h}) = N c_A c_B |f_A - f_B|^2 \times \{ I_{\mathrm{SRO}}(\mathbf{h}) + \mathbf{h} \cdot [\eta \mathbf{Q}^{AA}(\mathbf{h}) + \xi \mathbf{Q}^{BB}(\mathbf{h})] \}. \quad (3)$$

The prefactor $N c_A c_B |f_A - f_B|^2$ is one Laue unit (Lu) of the sample containing N atoms and $\eta = \mathrm{Re}\{f_A/(f_A - f_B)\}$, $\xi = \mathrm{Re}\{f_B/(f_A - f_B)\}$ are scattering factor ratios.

To determine the Fourier coefficients α_{lmn} and $\langle x_{lmn}^{\mu\mu} \rangle$ from diffuse x-ray scattering, the Georgopoulos–Cohen (GC) method and the 3λ method are employed. In the GC method, the inelastic scattering contributions are first calculated and subtracted. Then, the different symmetry of the 25 Fourier series and the different dependences of the scattering-factor ratios on the scattering vector are exploited to separate the Fourier series and to determine the Fourier coefficients hereafter. In the 3λ method, the quadratic displacement scattering with its 18 Fourier series is first subtracted together with the thermal diffuse scattering as they are experimentally accessible through the null-Laue measurement. Then, the Fourier coefficients are directly obtained by a least-squares fitting. Since calculated intensities must be subtracted from experimental intensities or experimental data sets must be compared, it is essential to obtain scattering intensities in absolute units.

III. EXPERIMENT

Starting from an alloy prepared from 99.99% Cu (Materials Research SA, München, Germany) and 99.99% Mn (Johnson Matthey GmbH, Karlsruhe, Germany), a single crystal of Cu-rich Cu-Mn was grown by the Bridgman technique. A slice with a ⟨421⟩ surface normal, 11.8 mm in diameter and 3 mm in thickness, was cut by spark erosion. The Mn fraction as determined by x-ray fluorescence was 17.2(2) at. %. The sample was homogenized at 1123 K for 24 h, water quenched, aged at 483 K in an oil bath for 2 weeks, and then water quenched. This treatment had been chosen to set up a state of thermal equilibrium[20] and is the same as previously employed in a diffuse neutron scattering experiment.[1] The surface was mechanically polished down to a SiC grain size of 5 μm and electro-wipe-polished using orthophosphoric acid.

Diffuse x-ray scattering was measured on beamline X14 at the NSLS (Brookhaven, USA). The beamline was equipped with a mirror focusing vertically and a Si(111) double-crystal monochromator which consisted of a flat crystal and a sagitally bent crystal for focusing in the horizontal plane. The incoming beam was set to 1 mm (vertical) × 1.5 mm (horizontal) by slits. The energy resolution amounted to about 1.3 eV.[21] Intensity was registered energy resolved using a mosaic crystal spectrometer.[22] Scattering at about 5500 positions was registered at $h_3 \leq h_2 \leq h_1$ positions within a range of scattering vectors of $0.5 < |\mathbf{h}| < 3.5$ on a simple cubic grid of 0.1 rlu. In addition, the intensities were registered on body-centered positions within a cube of an edge length of 0.5 rlu around $1\frac{1}{2}0$ positions, the location of the diffuse maxima. Three such data sets were collected, at 6526 eV (12 eV below the Mn K edge), 8969 eV (11 eV below the Cu K edge), and 8909 eV (71 eV below the Cu K edge).

Scattering intensities were registered with the energy-analyzing setup at a resolution of about 30 eV.[22] Strong resonant Raman scattering K-M_{II} M_{III} was only found at 8969 eV, not at 6526 eV where it did not manifest itself, in the presence of Compton scattering, even when moving into the absorption edge (Fig. 1). To separate elastic coherent scattering and thermal diffuse scattering (second peak) from resonant Raman scattering (first peak) and Compton scattering, several strategies were tried: (i) only employing intensities on the high-energy side of the second peak (i.e., beyond the peak maximum), (ii) taking the data beyond the dip between both peaks, (iii) using an intensity extrapolation from the first peak as "background" under the second peak, and (iv) using the intensity tails on the high-energy side of the second peak also on its low-energy side in a mirrored way. The latter three procedures yielded intensities that agreed with respect to the total average value within ±2% and had a standard deviation for all individual positions of typically 0.05. The first procedure suffered from the loss in counting statistics. Because of the different weights of Compton scattering and resonant Raman scattering at the three energies (see Fig. 1), different procedures were finally selected. Thermal diffuse and elastic coherent scattering off the Bragg positions amounted to ~2000–8000 counts at 6526 eV and ~10 000–20 000 counts at 8969 and 8909 eV; the counting

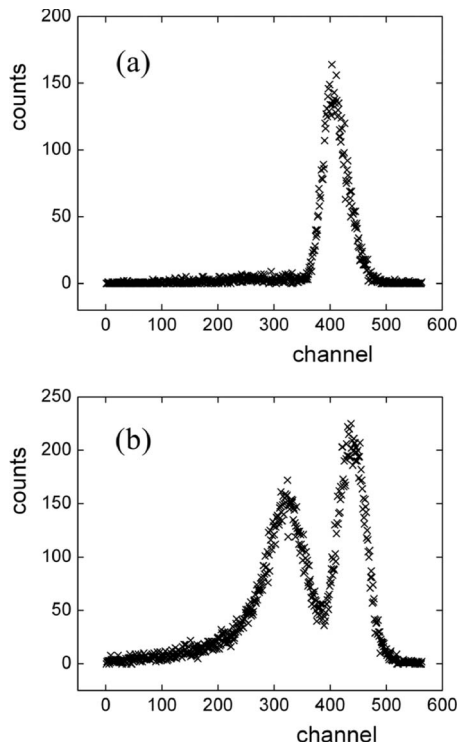

FIG. 1. Energy-resolved spectra as registered with the mosaic crystal spectrometer at $\mathbf{h}=(1.5,0,-1)$ using x rays of (a) 6526 eV and (b) 8969 eV in incoming energy. Elastic diffuse scattering and thermal diffuse scattering are located around the peak positions (a) ~410 and (b) ~440, respectively, with Compton scattering spread over lower channel numbers. Only at (b) 8969 eV, resonant Raman scattering leads to a well-resolved second peak.

time was 20–25 s. The data were corrected for background and the partial passing of the incident beam, as seen in the variation of the Mn K_β and Cu K_β fluorescence intensity with varying diffractometer settings.

Scattering was calibrated to absolute units by measuring the integrated intensity of the 111, 200, 220, 311, and 222 Debye–Scherrer rings of a well-defined Ni-powder standard.[23] Together with the Cu-Mn sample, the Ni standard was mounted under an evacuated Be hemisphere. The three data sets after calibration were found to be consistent among one another within less than 10%, when comparing the scattering close to the Bragg reflections (where thermal diffuse scattering of first order is expected to be predominant for a system with local order).

Atomic scattering factors were taken from Doyle and Turner,[24] and anomalous scattering factors as well as the linear absorption coefficients were taken from Sasaki.[25,26] Thermal diffuse scattering up to third order (required for the Georgopoulos–Cohen separation method) was calculated using the elastic constants as previously determined; $c_{11}=145(3)$ GPa, $c_{12}=105(3)$ GPa, and $c_{44}=73.8(8)$ GPa.[1] The overall (dynamic and static) B value ($=7.05\times10^{-3}$ nm^2) of the Debye–Waller factor $\exp[-2B(\sin\theta/\lambda)^2]$ was also taken from Roelofs *et al.*[1]

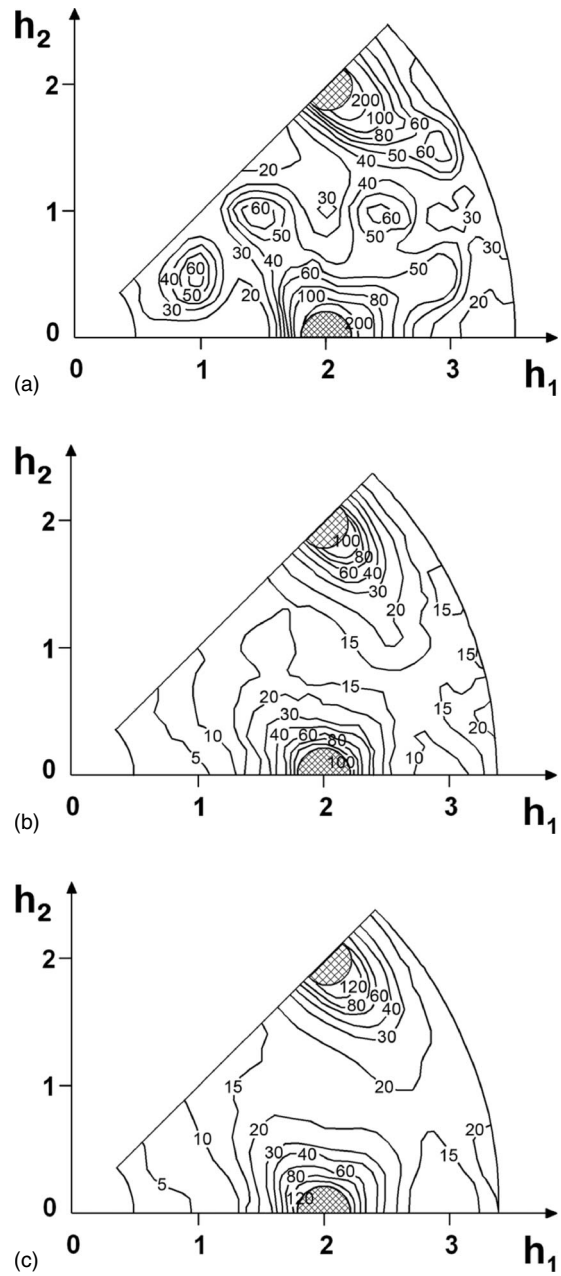

FIG. 2. Elastic coherent and thermal diffuse scattering in e.u. for the $(h_1,h_2,0)$ plane at (a) 6526 eV, (b) 8969 eV, and (c) 8909 eV.

IV. RESULTS

The diffuse scattering for $(h_1,h_2,0)$ positions is given in Fig. 2. The largest modulation at all three energies arises through thermal diffuse scattering close to the Bragg reflections. Modulations from elastic coherent diffuse scattering are only recognizable at 6526 eV, where the $1\frac{1}{2}0$ maxima from short-range order scattering are well resolved. This outcome is easily understood when one Laue unit is transferred to electron units (e.u.), the unit employed in Fig. 2; it amounts to 11.4 e.u. at 6526 eV, but only to 1.3 e.u. at 8969 eV and 0.5 e.u. at 8909 eV (values refer to position $\mathbf{h}=0$). For all the data evaluations, 40 values from previous small-angle neutron scattering (SANS) measurements[2,5] were added to the x-ray scattering data.

TABLE I. Warren–Cowley short-range order parameters α_{lmn} for the measurement at 6526 eV and the two (GC, 3λ) evaluations where data at all three energies were employed (SANS data from Refs. 2 and 5 were included). In comparison, the data from a previous neutron scattering measurement of Roelofs *et al.* (Ref. 1) are given.

	α_{lmn}			
lmn	GC 6526 eV	GC 6526, 8969, and 8909 eV	3λ	Neutrons
000	0.9514(202)	1.0015(121)	1.0299(37)	0.9630(15)
110	−0.0969(57)	−0.1081(47)	−0.0696(12)	−0.0970(4)
200	0.0741(63)	0.0945(43)	0.0784(15)	0.0870(5)
211	0.0398(33)	0.0524(22)	0.0460(8)	0.0441(3)
220	−0.0454(44)	−0.0422(27)	−0.0400(11)	−0.0391(4)
310	−0.0197(31)	−0.0272(22)	−0.0200(7)	−0.0220(3)
222	−0.0629(55)	−0.0706(34)	−0.0523(13)	−0.0543(5)
321	0.0279(23)	0.0255(16)	0.0213(5)	0.0201(2)
400	0.0568(66)	0.0524(44)	0.0379(14)	0.0433(6)
330	−0.0160(36)	−0.0189(30)	−0.0217(10)	−0.0202(4)
411	−0.0091(26)	−0.0071(22)	−0.0082(7)	−0.0061(3)
420	0.0121(30)	0.0080(21)	0.0055(7)	0.0046(3)
233	0.0049(28)	0.0048(23)	0.0037(7)	0.0025(3)
422	−0.0097(30)	−0.0088(20)	−0.0069(7)	−0.0086(3)
431	0.0068(18)	0.0053(14)	0.0035(5)	0.0018(2)
510	0.0041(29)	0.0026(26)	−0.0042(7)	−0.0047(3)
521	0.0095(16)	0.0075(14)	0.0065(5)	0.0051(2)
440	0.0118(46)	0.0108(27)	0.0058(10)	0.0015(4)
433		0.0031(23)	0.0025(7)	−0.0001(3)
530		−0.0028(18)	−0.0032(7)	−0.0035(3)
244		−0.0009(20)	−0.0003(7)	−0.0021(3)
600		0.0090(42)	0.0096(14)	0.0106(5)
532		0.0022(13)	0.0032(5)	0.0013(2)
611		−0.0002(20)	−0.0020(7)	−0.0012(3)
620		0.0062(20)	0.0040(7)	0.0024(3)

A. Georgopoulos–Cohen method

Thermal diffuse scattering was calculated up to third order and subtracted. In principle, one data set is sufficient to provide the Fourier coefficients α_{lmn} and $\langle x_{lmn}^{\mu\mu}\rangle$, most reliably from the data obtained with the largest scattering contrast (6526 eV). The low number of symmetry-equivalent positions close to the number of fitted contributions (25 in the general case) in the present measurement, however, will not allow $\langle x_{lmn}^{\mu\mu}\rangle$ to be determined. Still, the Warren–Cowley short-range order parameters, which are given in Table I for this measurement, agree well with the previous neutron scattering data of Roelofs *et al.*[1] In comparison with the x-ray measurements, neutron scattering benefitted from the experimental separation of thermal diffuse scattering and the much larger scattering contrast $2|f_{\mathrm{Cu}}-f_{\mathrm{Mn}}|/|f_{\mathrm{Cu}}+f_{\mathrm{Mn}}|$; its value is 5.7 with thermal neutrons and only 0.45 with x rays at 6526 eV (value for $\mathbf{h}=0$). The value of α_{000} is close to 1 as it should be.

For the combined evaluation of the three data sets, a fine-tuning of the calibration was done with respect to the measurement at 6526 eV. Such a recalibration was also noted to be required in previous 3λ investigations.[15,18] By taking thermal diffuse scattering close to Bragg reflections (within 0.25 rlu) as a reference and leaving the calibration at 6526 eV as given from the Ni-powder standard, the data at 8969 and 8909 eV have to be rescaled by 2% and 7%, respectively. The finally applied corrections were slightly larger (5% and 12%, respectively), but still consistent with an uncertainty of ±5% considered typical for conversion factors. With these corrections, α_{000} close to 1 is achieved for any combined evaluation of measurements at different energies. At all three energies, the ratio between the measured diffuse scattering and the calculated thermal diffuse scattering was larger than 1 (about 1.7). This larger value demonstrates that Huang scattering, which shows the same dependence on the scattering factors as thermal diffuse scattering, is also an important scattering contribution for the present alloy.

The large number of symmetry-equivalent positions (up to 130, i.e., twice the number usually employed) in a combined evaluation of the three data sets and the large variation of the scattering factor ratio η/ξ [Fig. 3(a)] were beneficial for a

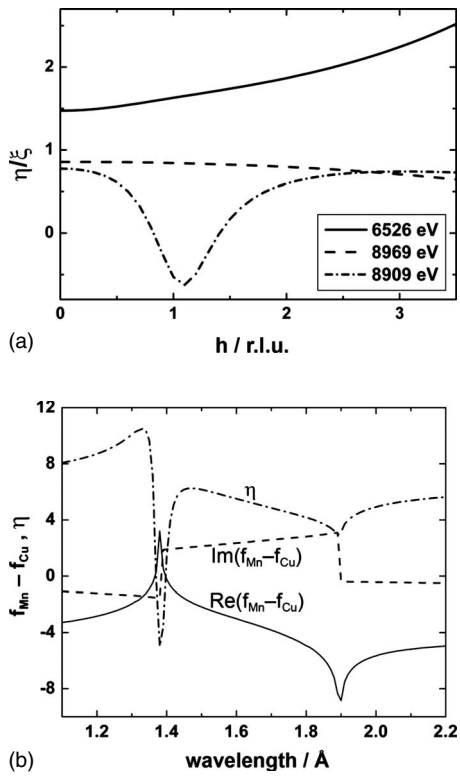

FIG. 3. (a) Variation of the atomic scattering factor ratio η/ξ [where $\eta=\mathrm{Re}\{f_{\mathrm{Cu}}/(f_{\mathrm{Cu}}-f_{\mathrm{Mn}})\}$ and $\xi=\mathrm{Re}\{f_{\mathrm{Mn}}/(f_{\mathrm{Cu}}-f_{\mathrm{Mn}})\}$] with the scattering vector $|\mathbf{h}|$ at 6526, 8969, and 8909 eV. (b) The wavelength dependence of the scattering contrast $f_{\mathrm{Mn}}-f_{\mathrm{Cu}}$ and of η are shown for $\mathbf{h}=0$.

good separation of the Fourier series. At two energies, η and ξ have the same sign, being positive at 6526 eV and negative at 8969 eV; thus, η/ξ is always positive. The change in sign of η/ξ at 8909 eV is easily understood if one considers the wavelength dependence of η [Fig. 3(b), also note $\xi=\eta-1$]; only if the real and the imaginary parts of $f_{\mathrm{Mn}}-f_{\mathrm{Cu}}$ are close to zero (i.e., for the condition of a null-Laue measurement), a negative sign in η/ξ may occur, and this also depends on the actual value of $f_{\mathrm{Mn}}-f_{\mathrm{Cu}}$ for the given scattering vector (see also Ref. 18).

Data within <0.2 rlu around any Bragg reflection were discarded. The separated short-range order scattering was fitted by $25\alpha_{lmn}$, with a weighted R value of 0.07 (Table I). The fits of the separated $\mathbf{Q}^{\mathrm{CuCu}}(\mathbf{h})$ and $\mathbf{Q}^{\mathrm{MnMn}}(\mathbf{h})$ Fourier series were performed with eight Fourier coefficients, with weighted R values of 0.12 and 0.42, respectively (Table II). The difference in the weighted R values of both fits is connected with the large standard deviation due to counting statistics amounting typically to ~20% and ~40%, respectively, in any value of these Fourier series.

B. 3λ evaluation

The measurement at 8909 eV was taken as a first approximation for the null-Laue data. The intensities for wavelengths $\lambda_{v=1,2}$, which correspond to 6526 and 8969 eV, were corrected for any noncontrast contribution by subtracting the null-Laue data (wavelength λ_3) scaled to the corresponding "gray" scattering amplitude squared,

$$\Delta I_{v3} = I_{\mathrm{diff},\lambda_v} - \frac{|c_{\mathrm{Mn}} f_{\mathrm{Mn},v} + c_{\mathrm{Cu}} f_{\mathrm{Cu},v}|^2}{|c_{\mathrm{Mn}} f_{\mathrm{Mn},3} + c_{\mathrm{Cu}} f_{\mathrm{Cu},3}|^2} I_{\mathrm{diff},\lambda_3}. \quad (4)$$

In subsequent iterations, the data at 8909 eV were corrected for short-range order scattering and linear displacement scattering to achieve agreement between the Fourier coefficients used for calculating these subtracted intensities and the fitted Fourier coefficients. The least-squares fitting had a weighted R value of 0.24 (Tables I and II).

In comparison with the previous Georgopoulos–Cohen evaluation of the three data sets, the standard deviations of the Warren–Cowley short-range order parameters within the 3λ method are lower and a larger number of static atomic

TABLE II. Static atomic displacements $\langle x_{lmn}^{\mathrm{CuCu}}\rangle$, $\langle x_{lmn}^{\mathrm{MnMn}}\rangle$, and $\langle x_{lmn}^{\mathrm{CuMn}}\rangle$ (in units of the lattice parameter) for the two combined (GC, 3λ) evaluations.

	$\langle x_{lmn}^{\mathrm{CuCu}}\rangle$		$\langle x_{lmn}^{\mathrm{MnMn}}\rangle$		$\langle x_{lmn}^{\mathrm{CuMn}}\rangle$	
lmn	GC	3λ	GC	3λ	GC	3λ
110	−0.00256(5)	−0.00232(2)	−0.0392(22)	−0.0318(10)	0.00720(14)	0.00720(8)
200	0.00170(19)	0.00156(4)	0.0027(30)	0.0091(9)	−0.00506(73)	−0.00555(17)
211	−0.00007(4)	−0.00011(9)	0.0013(7)	0.0002(1)	−0.00001(13)	0.00026(23)
121	−0.00010(4)	−0.00075(7)	0.0008(7)	−0.0002(1)	0.00014(13)	0.00194(18)
220	−0.00082(7)	−0.00070(2)	−0.0118(19)	−0.0060(7)	0.00282(22)	0.00209(7)
310	−0.00009(5)	−0.00015(9)	0.0013(12)	−0.0001(1)	0.00010(15)	0.00036(21)
130	0.00006(5)	−0.00061(9)	0.0003(14)	−0.0004(1)	−0.00017(17)	0.00147(21)
222	−0.00038(6)	−0.00059(2)	0.0028(19)	−0.0048(5)	0.00067(18)	0.00169(6)
321		0.00014(6)		0.0000(1)		−0.00035(15)
231		−0.00044(6)		−0.0001(1)		0.00110(15)
132		0.00017(6)		0.0000(1)		−0.00042(15)
400		0.00046(4)		0.0030(12)		−0.00154(18)
330		−0.00029(2)		−0.0025(6)		0.00090(7)

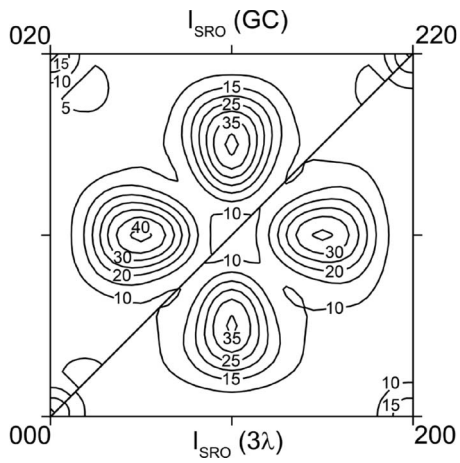

FIG. 4. Short-range order scattering $10\times I_{SRO}(\mathbf{h})$ for the (001) plane recalculated from the Fourier coefficients of Table I for the GC and 3λ evaluations.

displacements is determined. Both advantages come from the present one-step procedure in obtaining the Fourier coefficients, which is in contrast to the additional intermediate step of separating the Fourier series in the Georgopoulos–Cohen analysis. This was checked by a type of Georgopoulos–Cohen analysis (now comprising only the seven Fourier series of short-range order scattering and linear displacement scattering) of the same data as used in the 3λ analysis.

Figures 4 and 5 show the scattering contributions $I_{SRO}(\mathbf{h})$ and $\mathbf{h}\cdot\mathbf{Q}^{\mu\mu}(\mathbf{h})$, which are recalculated from the data sets of Tables I and II for both evaluation schemes. A kind of redistribution among the scattering contributions between both schemes is recognizable; modulations in $I_{SRO}(\mathbf{h})$ are larger with the Georgopoulos–Cohen scheme, while they are weaker with linear displacement scattering. This redistribution may not be attributed to a selected range of reciprocal space as, e.g., the maximum of $I_{SRO}(\mathbf{h})$ occurs at a location where linear displacement scattering amounts to 0 Lu due to symmetry reasons.

V. DISCUSSION

Tables I and II reveal some differences in the fitted Fourier coefficients beyond one standard deviation between both evaluation schemes for the present x-ray investigation. However, by considering the data of α_{lmn} and $\gamma_{x,lmn}$ from previous neutron scattering experiments as a reference, there seems to be no clear indication of the Georgopoulos–Cohen method to be preferred over the 3λ evaluation scheme or vice versa, as differences are minute.

A. Short-range order scattering

All the Warren–Cowley short-range order parameters of a given shell *lmn* in Table I agree in sign up to shell 510. Positive values of α_{l00} are obtained, which reflect the formation of short chains of Mn atoms along $\langle h00\rangle$. If one does not include the SANS data in the data evaluation, the Georgopoulos–Cohen separation scheme and the 3λ evaluation still show a (somewhat smaller) increase toward the direct beam (of 1.4–1.65 Lu, instead of ~2.0 Lu). The Warren–Cowley short-range order parameters will still agree within one standard deviation, while the displacement parameters remain (within <0.1 standard deviations) unaffected. A similar increase of up to ~1.5 Lu toward the direct beam was also obtained in a previous investigation combining diffuse neutron scattering at wide and small angles.[3]

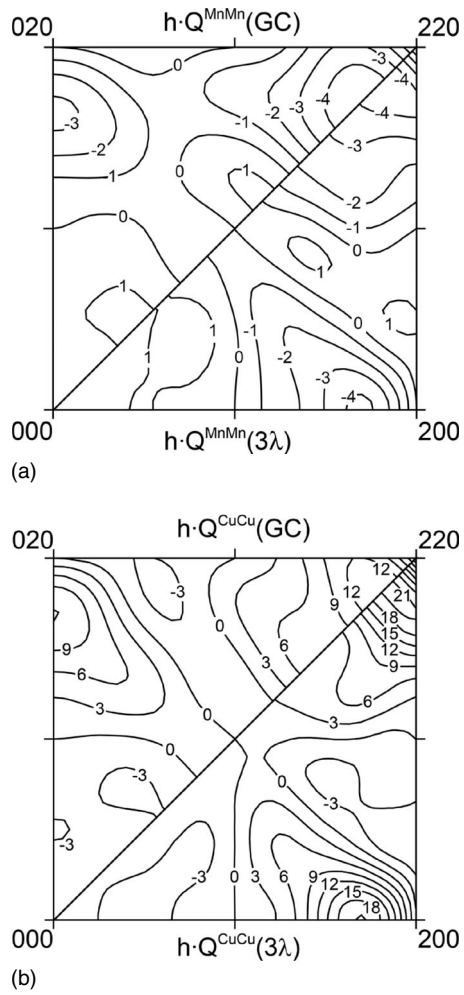

FIG. 5. Recalculated contributions (a) $10\times\mathbf{h}\cdot\mathbf{Q}^{MnMn}(\mathbf{h})$ and (b) $10\times\mathbf{h}\cdot\mathbf{Q}^{CuCu}(\mathbf{h})$ for the (001) plane using the Fourier coefficients of Tables I and II for the GC and 3λ evaluations.

B. Linear displacement scattering

For the static atomic displacements $\langle x_{lmn}^{\mu\mu}\rangle$, the sign and magnitude of the parameters closely agree between the two evaluations, except for two cases where a neighboring shell exhibits different x,y,z components ($\neq 0$). Examining the "simple" shells that are characterized by one component $\langle x_{lmn}^{\mu\nu}\rangle \neq 0$, one notices an expansion of the average lattice between those elements that are preferred over a random arrangement in site occupancy; i.e., positive values of $\langle x_{lmn}^{CuMn}\rangle$ are found for $lmn=110$, 220, 222, and 330 and positive values of $\langle x_{lmn}^{CuCu}\rangle$ and $\langle x_{lmn}^{MnMn}\rangle$ for $lmn=200$ and 400.

TABLE III. Effective displacements $\gamma_{x,lmn}$ for the two combined (GC, 3λ) evaluations. In comparison, the data from a previous neutron scattering measurement of Roelofs *et al.* (Ref. 1) are given.

	$\gamma_{x,lmn}$		
lmn	GC	3λ	Neutrons
110	0.0591(11)	0.0556(5)	0.0306(2)
200	−0.0371(45)	−0.0377(9)	−0.0254(5)
211	0.0007(9)	0.0023(18)	−0.0049(3)
121	0.0016(8)	0.0155(14)	0.0002(2)
220	0.0206(15)	0.0163(5)	0.0121(3)
310	0.0014(11)	0.0032(18)	0.0028(2)
130	−0.0014(12)	0.0126(18)	0.0018(2)
222	0.0069(13)	0.0134(4)	0.0117(3)
321		−0.0028(12)	−0.0028(2)
231		0.0092(12)	−0.0004(2)
132		−0.0035(12)	−0.0009(2)
400		−0.0108(10)	−0.0115(5)
330		0.0068(5)	0.0055(3)

According to the Froyen–Herring theory,[27] $\langle x_{lmn}^{AA}\rangle$ and $\langle x_{lmn}^{BB}\rangle$ of an *A*-*B* alloy should differ in sign. This conclusion was reached on the basis of two assumptions: (i) there is a random alloy and (ii) the nearest-neigbor force is species independent. Certainly, with α_{110} amounting to ~43% of the maximum magnitude of $1-1/0.828=-0.208$, assumption (i) is violated. However, even at lower degrees of local order or decomposition, no unique situation is met. While the sign prediction is violated with Fe-47 at. % Cr (α_{111} amounts to ~16% of the maximum magnitude[17]), it is fulfilled with Fe-36.8% at. % Ni (α_{110} amounts to ~10% of the maximum magnitude[16]). It seems plausible that assumption (ii) is not valid and that this might be the reason for the unpredictable sign behavior.

A judgment of the static atomic displacements is achieved by calculating the $\gamma_{x,lmn}$ only accessible in a single neutron scattering experiment which are given by

$$\gamma_{x,lmn} = -\frac{b_{\mathrm{Mn}}}{b_{\mathrm{Mn}}-b_{\mathrm{Cu}}}2\pi\left(\frac{c_{\mathrm{Mn}}}{c_{\mathrm{Cu}}}+\alpha_{lmn}\right)\langle x_{lmn}^{\mathrm{MnMn}}\rangle + \frac{b_{\mathrm{Cu}}}{b_{\mathrm{Mn}}-b_{\mathrm{Cu}}}2\pi\left(\frac{c_{\mathrm{Cu}}}{c_{\mathrm{Mn}}}+\alpha_{lmn}\right)\langle x_{lmn}^{\mathrm{CuCu}}\rangle. \quad (5)$$

Here, the $\langle x_{lmn}^{\mu\mu}\rangle$ are taken from Table II, and the coherent scattering lengths of thermal neutrons are $b_{\mathrm{Cu}}=7.718(4)$ fm and $b_{\mathrm{Mn}}=-3.73(2)$ fm.[28] Irrespective of the evaluation scheme and also in agreement with the previous neutron scattering experiments,[1,3] Table III shows large negative values for *l*00 neighboring shells and large positive values for the *ll*0 shells. Values from x-ray scattering turn out to be larger in magnitude than those from neutron scattering (this may be due to not completely balanced scattering contributions), which leads to larger modulations in linear displacement scattering.

No additional criterion for data quality is supplied from extended x-ray absorption fine structure (EXAFS) investigations as differences between both evaluation schemes are too small in the present case. For the case of a dilute solution (Cu-1 at. % Mn to work within the single-defect approximation), Scheuer and Lengeler[29] obtained $\langle\delta_{110}^{\mathrm{CuMn}}\rangle=0.020(10)$ and 0.016(20) Å depending on the model compound employed in the evaluation. First-principle studies[30] performed for dilute alloys of Cu-(0.5–0.7) at. % Mn yielded $\langle\delta_{110}^{\mathrm{CuMn}}\rangle=0.013-0.018$ Å. In both cases, the sign and magnitude are comparable with the present results of $\langle\delta_{110}^{\mathrm{CuMn}}\rangle=0.0375(7)$ Å (to obtain the radial displacements $\langle\delta_{110}^{\mathrm{CuMn}}\rangle$, the axial displacement components $\langle x_{110}^{\mathrm{CuMn}}\rangle$, which are given in Table II, were multiplied by $\sqrt{2}a$).

TABLE IV. Static atomic displacements $\langle x_{lmn}^{\mathrm{CuMn}}\rangle$ (in units of the lattice parameter) for the 3λ evaluation and for the dilute limit of Mn in Cu in a macroscopic and microscopic approach (Ref. 10).

		$\langle x_{lmn}^{\mathrm{CuMn}}\rangle$ dilute limit	
lmn	3λ	Macroscopic	Microscopic
110	0.00720(8)	0.0157	0.032(6)
200	−0.00555(17)	−0.0018	0.008(6)
220	0.00209(7)	0.0039	
222	0.00169(6)	0.0045	
400	−0.00154(18)	−0.0005	
330	0.00090(7)	0.0017	

With respect to the nearest-neighbor distance between Cu-Cu pairs, one obtains 2.593(1) Å, which is still larger than the value of 2.556 Å in pure Cu. Also, the nearest-neighbor distance between Mn-Mn pairs of 2.471(13) Å is still larger than the smallest value of 2.26 Å in pure Mn.[31]

Assuming that a single type of defect is present and that atomic displacements can be written as a linear superposition of the displacements corresponding to the individual fluctuation waves, the Fourier transform of the static displacement, $\mathbf{u}(\mathbf{h})$, is connected with the Fourier transform of the defect concentration, $c(\mathbf{h})$, by $\mathbf{u}(\mathbf{h})=\mathbf{A}(\mathbf{h})c(\mathbf{h})$ and may be calculated within a continuum or an atomistic model.[10] To attribute a species dependence to $\mathbf{u}(\mathbf{h})$ and to rely on easily accessible experimental data (such as the lattice parameter change with composition and the elastic constants), the case of dilute Mn impurities within a Cu matrix was considered and the static displacements $\langle x_{lmn}^{\mathrm{CuMn}}\rangle$ were estimated in two ways. (i) Using the elastic data $c_{11}=170$ GPa, $c_{12}=122.5$ GPa, and $c_{44}=75.8$ GPa of Cu (Ref. 32) and a lattice parameter change with composition of 0.10 for Mn in Cu, atomic displacements were determined taking into account the elastic anisotropy $\xi=(c_{11}-c_{12}-2c_{44})/c_{44}$ according to Krivoglaz.[10] (ii) In an atomistic approach, the nearest-neighbor Kanzaki forces (see, e.g., Kostorz[33] and references therein), determined to be 1.2 eV/Å from c_{ij} and the lattice parameter change with composition,[10] and the Green's function as given by Martinsen[34] for Cu were employed to obtain $\langle x_{lmn}^{\mathrm{CuMn}}\rangle$. Table IV shows that the signs and order of magnitude of the experimental displacements are approximately met. As one type of any two static atomic displacements seems reproduced, there is no compelling reason to doubt the magnitude and sign of the data in Table II.

The data sets of Ni-Fe,[15] Ni-Cr (Ref. 18) [note that only the 3λ evaluation yielded the same sign for nearest-neighbor Ni-Cr displacements of $\langle \delta_{110}^{\mathrm{NiCr}} \rangle = -0.0034$ Å as the EXAFS investigation[29] of Ni-2.46 at. % Cr with −0.11(7) Å], and Fe-Cr (Ref. 17) showed in common that the preferred nearest-neighbor pairs have a shortened bond distance. This is no longer fulfilled with Cu-Mn. Still in all four systems investigated, the lattice parameter showed a clear increase when adding a second component. There is only one striking difference among these systems; no intermetallic phase is known for Cu-Mn.

VI. CONCLUSION

From the present investigation, it may be concluded that a successful analysis of species-dependent static atomic displacements may also be done with alloys where the constituents are further apart in the periodic table than just by a difference of 2 in the atomic numbers. The discrepancies, which were previously observed when applying the two evaluation schemes with Ni-Cr,[18] may be correlated with the closeness to the absorption edges where the experiments were performed; while it amounted to 6 eV below the Ni *K* edge, energies of 10–20 eV below absorption edges were chosen in the other 3λ investigations. The present results may provide useful input for further theoretical work to better understand static displacements. For systems where no null-Laue measurement can be performed, two investigations close to the absorption edges of the constituents will be very helpful for a robust determination of the static displacements, despite the crucial point of a common data calibration.

ACKNOWLEDGMENTS

The authors are grateful to E. Fischer for his support in growing the single crystal. This work was partially supported by the "Schweizerischer Nationalfonds zur Förderung der wissenschaftlichen Forschung". The research was performed at the ORNL beamline X14 at the NSLS, BNL, which was sponsored by the Division of Materials Sciences and Division of Chemical Sciences, U.S. Department of Energy, and under Contract No. DE-AC05-840R21400 with UT-Batelle.

*Present address: Swiss Steel AG, 6020 Emmenbrücke, Switzerland.

[1] H. Roelofs, B. Schönfeld, G. Kostorz, and W. Bührer, Phys. Status Solidi B **187**, 31 (1995).
[2] B. Schönfeld, O. Paris, G. Kostorz, and J. Skov Pedersen, J. Phys.: Condens. Matter **10**, 8395 (1998).
[3] B. Schönfeld, R. Bucher, G. Kostorz, and M. Zolliker, Phys. Rev. B **69**, 224205 (2004).
[4] H. Reichert, V. N. Bugaev, O. Shchyglo, A. Schöps, Y. Sikula, and H. Dosch, Phys. Rev. Lett. **87**, 236105 (2001).
[5] B. Schönfeld, M. J. Portmann, G. Kostorz, and J. Kohlbrecher, Phys. Rev. B **66**, 100102(R) (2002).
[6] T. Gödecke, Z. Metallkd. **81**,826(1990).
[7] P. Wells and J. H. Smith, J. Phys. F: Met. Phys. **1**, 763 (1971).
[8] M. Hirabayashi, M. Koiwa, S. Yamaguchi, and K. Kamata, J. Phys. Soc. Jpn. **45**, 1591 (1978).
[9] J. W. Cable, S. A. Werner, G. P. Felcher, and N. Wakabayashi, Phys. Rev. B **29**, 1268 (1984).
[10] M. A. Krivoglaz, *X-Ray and Neutron Diffraction in Nonideal Crystals* (Springer, Berlin, 1995).
[11] J. A. Rodriguez, S. C. Moss, J. L. Robertson, J. R. D. Copley, D. A. Neumann, and J. Major, Phys. Rev. B **74**, 104115 (2006).
[12] P. Georgopoulos and J. B. Cohen, J. Phys. Colloq. **38**, C7-191 (1977).
[13] B. Borie and C. J. Sparks, Jr., Acta Crystallogr., Sect. A: Cryst. Phys., Diffr., Theor. Gen. Crystallogr. **27**, 198 (1971).
[14] G. E. Ice, C. J. Sparks, A. Habenschuss, and L. B. Shaffer, Phys. Rev. Lett. **68**, 863 (1992).
[15] X. Jiang, G. E. Ice, C. J. Sparks, L. Robertson, and P. Zschack, Phys. Rev. B **54**, 3211 (1996).
[16] J. L. Robertson, G. E. Ice, C. J. Sparks, X. Jiang, P. Zschack, F. Bley, S. Lefebvre, and M. Bessiere, Phys. Rev. Lett. **82**, 2911 (1999).
[17] L. Reinhard, J. L. Robertson, S. C. Moss, G. E. Ice, P. Zschack, and C. J. Sparks, Phys. Rev. B **45**, 2662 (1992).
[18] B. Schönfeld, G. E. Ice, C. J. Sparks, H.-G. Haubold, W. Schweika, and L. B. Shaffer, Phys. Status Solidi B **183**, 79 (1994).
[19] B. Schönfeld, Prog. Mater. Sci. **44**, 435 (1999).
[20] R. Reihsner and W. Pfeiler, J. Phys. Chem. Solids **46**, 1431 (1985).
[21] A. Habenschuss, G. E. Ice, C. J. Sparks, and R. A. Neiser, Nucl. Instrum. Methods Phys. Res. A **266**, 215 (1988).
[22] G. E. Ice and C. J. Sparks, Jr., Nucl. Instrum. Methods Phys. Res. A **291**, 110 (1990).
[23] P. Suortti and L. D. Jennings, Acta Crystallogr., Sect. A: Cryst. Phys., Diffr., Theor. Gen. Crystallogr. **33**, 1012 (1977).
[24] P. A. Doyle and P. S. Turner, Acta Crystallogr., Sect. A: Cryst. Phys., Diffr., Theor. Gen. Crystallogr. **24**, 390 (1968).
[25] S. Sasaki, KEK Report No. 88-14, KEK, Tsukuba, Japan, 1989 (unpublished).
[26] S. Sasaki, KEK Report No. 90-16, KEK, Tsukuba, Japan, 1990 (unpublished).
[27] S. Froyen and C. Herring, J. Appl. Phys. **52**, 7165 (1981).
[28] V. F. Sears, Neutron News **3**, 26 (1992).
[29] U. Scheuer and B. Lengeler, Phys. Rev. B **44**, 9883 (1991).
[30] N. Papanikolaou, R. Zeller, P. H. Dederichs, and N. Stefanou, Phys. Rev. B **55**, 4157 (1997).
[31] J. A. Oberteuffer and J. A. Ibers, Acta Crystallogr., Sect. B: Struct. Crystallogr. Cryst. Chem. **26**, 1499 (1970).
[32] Y. A. Chang and L. Himmel, J. Appl. Phys. **37**, 3567 (1966).
[33] G. Kostorz, in *Physical Metallurgy*, 4th ed., edited by R. W. Cahn and P. Haasen (North-Holland, Amsterdam, 1996), p. 1115.
[34] D. Martinsen, KFA Jülich Report No. 1508, KFA, Jülich, Germany, 1978 (unpublished).